PET reconstruction of posterior image probability including anatomical information

Marina Filipovic[1], Eric Barat[2], Thomas Dautremer[2], Claude Comtat[1], and Simon Stute[1]

[1]IMIV, CEA, Inserm, CNRS, Univ. Paris Sud, Université Paris Saclay, CEA-SHFJ, Orsay, France
[2]CEA, LIST, Laboratory of Systems Modelling and Simulation, Gif-sur-Yvette, France

I. INTRODUCTION

Most iterative PET reconstruction methods are based on formulating a function relating the observed acquired data to the unknown emission image. The reconstructed image represents either the zero, the minimum, or the maximum of this function: it is found using different numerical optimization methods and may not be unique. A thourough review of existing iterative methods can be found in Qi and Leahy [7].

Usually, the observed acquired data are modeled as a random variable, where the randomness comes from the noise or from unwanted signals, and the image is regarded as deterministic and fixed. This is the case for MLEM and its variations. As PET reconstruction is an ill-posed inverse problem, and rather challenging to solve, some methods introduce additional constraints and prior assumptions which can drive the final solution into some desirable directions. These methods have two theoretical interpretations leading to equivalent algorithms: 1) the image is regarded as deterministic, but a penalty term is added to the function (penalized maximum likelihood) 2) the image is regarded as a random variable, and the solution represents the maximum of the posterior distribution (MAP or maximum a posteriori). These methods have been used extensively for introducing assumptions about local smoothness in the image and for integrating anatomical information from other modalities into PET images. Integration of supplementary anatomical information into PET reconstruction may cause improvements in spatial resolution, partial volume issues, bias-variance performance, etc. A thorough review of anatomically aided PET reconstruction methods and of their added value to PET images can be found in Bai et al. [2].

Only a few methods have explored more in depth the random nature of these models, by trying to recover entire posterior probability distributions (Higdon et al. [5], Weir [10], Barat et al. [3], Sitek [8]).

There are several advantages of estimating the entire posterior probability distribution instead of a single solution for the image: the posterior distribution reflects the uncertainty of the observed data, and intervals on this distribution (credible intervals) can be either used for interpretation or for statistical tests.

In this paper, we present a probabilistic reconstruction model that seeks to infer the entire posterior probability distribution of emission concentration in the imaged object, given observed acquired PET and coregistered anatomical multimodal data. It is based on the Bayes theorem, though we avoid using the label Bayesian because it has different meanings in different contexts and can be confusing. The prior is a distance-dependent Chinese Restaurant Process, presented in Blei and Frazier [4], and the posterior distribution is estimated by sampling.

II. METHODS

1. Theory

We use all the usual assumptions of MLEM and MAP (Poisson likelihood, introduction of complete data, system matrix and additive contribution of random and scattered counts). The novelties consist of building a sampler for the full posterior distribution, and of placing a distance-dependent Chinese Restaurant Process (ddCRP) prior on the image, [4]. This prior models a segmentation of the image into groups of voxels (segments) which are likely to have the same intensity, and includes a prior on segment intensity (each segment having uniform intensity). Observed information about segment intensities comes only from PET data, but observed information about local uniformities can be supplied by as many sources as available. Anatomical (MRI) data are therefore used to pro-

DOI: 10.12059/Fully3D.2017-11-3104002

vide more side information about segmentation probabilities.

Let y_i be the observed number of counts acquired in the line of response (LOR) i, n_{ij} the complete data (number of counts emitted in voxel j and detected in LOR i), A_{ij} elements of the system matrix, λ_s the emission concentration [Bq/volume] not per voxel but per uniform segment, and c the segmentation of the image into groups of voxels with the same emission concentration (implemented through links between neighbouring voxels). The prior on segment intensity is chosen to be a Gamma distribution, for several practical and realistic reasons: the Gamma distribution has the convenient property of being the conjugate prior for Poisson distribution (the posterior distribution can be easily expressed analytically), it is non negative and very versatile (various emission distributions as well as less informative distributions can be approximated by choosing appropriate parameters).

The PET image being thus modeled with both intensity λ and segmentation c, the posterior distribution for our model is $p(\lambda, c, n|y)$ and it is estimated by sampling. We built a MCMC Gibbs sampler, which requires the following conditional probabilities:

1 - The complete data conditional probability is derived directly from usual PET assumptions. It is a multinomial distribution with y_i trials, the outcomes being the voxels and the additive random/scatter signal q_i. Outcome probabilities are determined using the system matrix and the random/scatter expectation $\bar{q}_i$, as :

$$\frac{A_{ij}\lambda_j}{\sum_k A_{ik}\lambda_k + \bar{q}_i}, \qquad \frac{\bar{q}_i}{\sum_k A_{ik}\lambda_k + \bar{q}_i} \tag{1}$$

for voxels (left) and random/scatter contribution (right).

2 - The ddCRP segmentation conditional probability is implemented with another Gibbs sampler presented in [4]. The required conditional probabilities are the probabilities for each voxel of being linked to one of its neighbours, given the current links of all the other voxels and given the observed data. In this study, we used an MRI image to provide information about uniform segments. The MRI image is modeled rather simply, with a Gaussian distribution and with additive Gaussian noise.

3 - Segment intensity conditional probability is a Gamma distribution expressed per segment s, derived from Gamma-Poisson conjugate pair. Its expectation is proportional to the ratio of the sum of all n_{ij} for the segment and the sum of all voxel sensitivities for the segment. The influence of the Gamma segment intensity prior is rather explicit: the parameters of the prior (shape parameter a and rate parameter b) are added to the previously described sums. Their influence decreases when segment size or quantity of observations increase, and their influence will be strongest for single voxel segments with few observed counts.

$$p(\lambda_s|n_{j\in s}) = Gamma(\sum_{j\in s}\sum_i n_{ij} + a, \sum_{j\in s} sens_j + b) \tag{2}$$

There are several possibilities for choosing an image estimator from a probability distribution. In this study we focused on posterior expectation, estimated by averaging the samples. The final image represents therefore an average of likely segmentations and likely segment intensities.

2. Implementation and validation

First, simulations were run in order to perform extensive quantitative tests. All the reconstructions were implemented using the CASToR library in C++, [1].

An MRI T1 brain image with associated label image was generated from the BrainWeb database. We used realistic FDG PET values for a healthy brain to generate a PET image from the label image. The MRI and the PET image were thus perfectly registered, but some edges were slightly blurred in the MRI image due to its realistic nature. In order to further test edge mismatches, we added a hyperintense lesion in the PET image but not in the MRI. In-house analytical simulation library, Stute et al. [9], was used to simulate 100 replicates of realistic PET observations, with $5e^6$ prompts ($\sim 2.5e^6$ true counts) for a 2D slice and $7e^7$ prompts for 3D data, using Siemens Biograph PET/CT geometry, and including attenuation, random and scatter counts, resolution modeling (PSF blurring), etc. There was no PSF modeling in the reconstructions. Quantitative analysis on replicates was done on 2D data because of the required computation time, and 3D data were reconstructed with the same parameters for a single replicate. The Gibbs sampler was iterated 1000 times, but as it had difficulties converging to the final distribution, we ran it several times (here 35), and took the last 100 samples from each run.

Regarding the Gamma prior on segment intensity, we tested several approaches for fixing the shape and rate parameters : using an estimation of intensity expectation from the observed data, and using approximations of non-informative priors (uniform prior and Jeffreys non-informative prior for Poisson likelihood, Jeffreys [6]). As the results were rather similar for different intensity

priors, only the results with the approximate non-informative Jeffreys prior are presented.

The ddCRP contains an internal parameter which affects to some extent segment sizes, [4]: it was chosen empirically.

The performance and the characteristics of the new reconstruction were analyzed using several methods. The new image estimator (the posterior mean) was compared with raw and post-smoothed converged MLEM estimator in terms of bias, variance and root mean square error over 100 replicates. MLEM post-smoothing was done with a Gaussian filter with FWHM equal to the blurring of the PET acquisition system. As voxel-wise analysis is rather difficult because of high noise and variance, especially in MLEM, regions of interest were selected in the simulated true image according to region uniformity, edges and type of intensity (hyperintense lesion, hypointense cerebro-spinal fluid (CSF) surrounded by gray matter, portion of gray matter (GM)). 95% intervals were computed both on voxel-wise distributions over replicates for all estimators (approximation of confidence intervals), and on the posterior distribution obtained with the new method for each replicate (credible intervals). Their coverage of the true values was observed over brain voxels, as neither method is capable of obtaining true zero values in the background. It should be noted that these two types of intervals do not have equivalent meanings, and cannot be directly compared.

Second, patient 3D brain data were obtained from a GE PET/MRI scanner, from an approved research protocol EPIPED. The T1 3D MRI image was resampled to match the voxel size of the reconstructed PET image. Two values were chosen for the transaxial size of reconstructed voxels, 2.3mm and 1mm, the first being suitable for MLEM reconstruction without PSF modeling and without TOF, and the second being too low. Algorithm parameters for the new method were the same as for the simulated data, except that the Gibbs sampler was rerun 30 times with 250 iterations per run.

III. RESULTS

Simulated PET and MRI images are shown in Fig.1, and reconstructed images (2D and the same slice in 3D) are shown in Fig.2 for the proposed method and for raw and post-smoothed converged MLEM (all the PET images are scaled with the same color map as the phantom in Fig.1).

In the new reconstruction, the edges are well defined and overlap well with the edges in the true image, which can be interpreted as an improvement of spatial resolution. Some edges that do not exist in the MRI image are less visible in the reconstructed image, for instance the lower edge of the lesion. Image areas that have uniform intensity in the true image approach uniformity also in the reconstructed image. Fig.3 shows identically scaled images of absolute bias over replicates of the new estimator and MLEM : it is clear that the bias at the edges is lower with our method. Considering the whole image, the new method presents slightly lower bias and lower variance compared to converged MLEM, and lower bias and slightly lower variance compared to post-smoothed MLEM. The new method reduces the root mean square error computed over the whole image by 72% compared to converged MLEM.

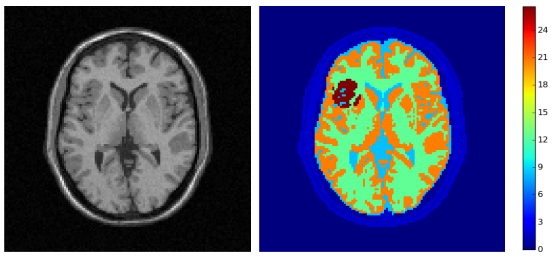

Figure 1: *Simulated MRI and PET images*

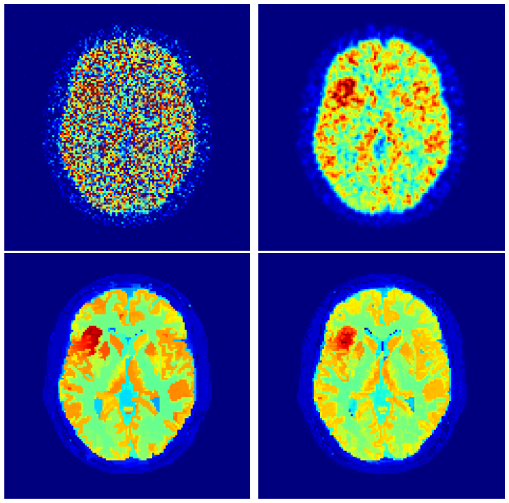

Figure 2: *Up: converged and post-smoothed MLEM Down: new method 2D and 3D (same color scale as phantom Fig.1)*

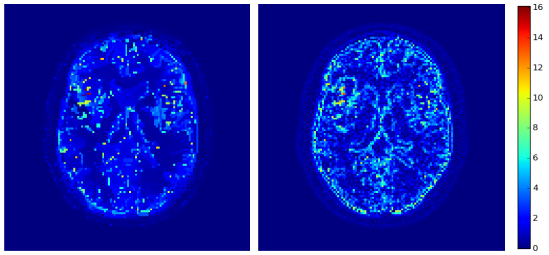

Figure 3: *Estimator bias for the new method (left) and converged MLEM (right)*

Fig.4 presents bias-standard deviation plots for the selected regions of interest, for the new method, converged and post-smoothed MLEM. Lower and upper limits of 95% intervals are also displayed. As to the regions of interest, the new method presents roughly similar bias and lower variance compared to converged MLEM, and lower bias and similar variance compared to post-smoothed MLEM. For all methods, the hyperintense lesion and gray matter are underestimated, and the hypointense region surrounded by gray matter is overestimated.

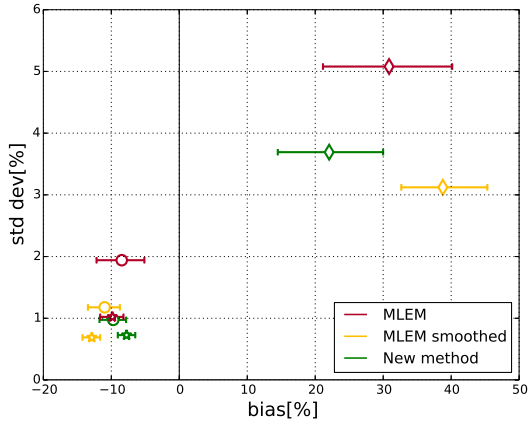

Figure 4: *Estimator bias-standard deviation comparison for ROIs : lesion(○), CSF(◇), GM(∗)*

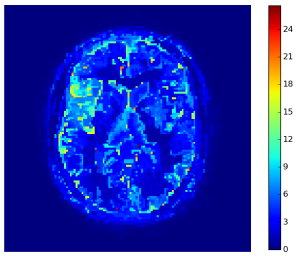

Figure 5: *Image of credible intervals*

The posterior distribution per replicate presents rather tight (credible) intervals, partly because anatomical MRI information lowers the uncertainty about the segmentation part of the model. Fig.5 shows an image of the absolute size (maximum - minimum) of credible intervals for one replicate: areas with larger intervals tend to match areas in the reconstructed image where the intensities differ more from the true image. Estimator intervals, computed over estimator distributions, had a coverage of true values over brain voxels of 100% for converged MLEM, 82% for smoothed MLEM, and 32% for the new method. Credible intervals, computed per replica over the posterior distribution obtained with the new method, had a 60% coverage of true values over brain voxels, in average over replicates. This lower coverage is probably caused by the combined properties of noteworthy bias and low variance of the new method.

Regarding patient data, Fig.6 shows the MRI image at smaller voxel size and the converged post-smoothed MLEM reconstruction at larger voxel size. Fig.7 shows reconstructions with the new method, both the posterior mean image and the credible intervals image, for smaller and larger voxel size. The reconstructed images present sharper edges and more details. The color scale is identical for MLEM and the posterior mean image, the unit being Bq/ml.

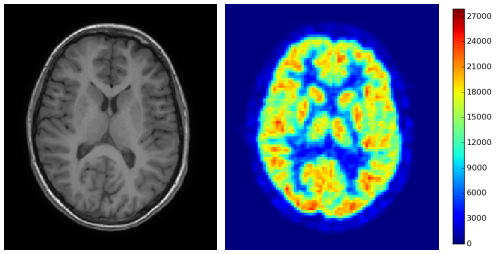

Figure 6: *Patient MRI and post-smoothed MLEM*

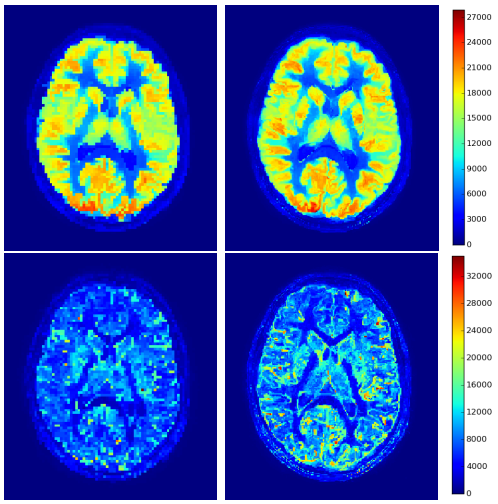

Figure 7: *New method mean (up) and interval (down) image at larger (left) and smaller (right) voxel size*

IV. DISCUSSION

The lack of system resolution modeling in the reconstruction has probably slightly impaired the effect of registration between the MRI and the PET. PSF modeling will be introduced in a probabilistic manner in the model. TOF management will be implemented as well, as it is expected to improve the results and to aid sampler convergence. This feature will be especially useful for patient

data, as TOF information is available for out PET/MRI scanner.

The MRI image does not affect the PET image intensity directly, it only influences the segmentation part of the model. It should be noted that there is no final piece-wise segmentation of the image: the segmentation occurs only in individual samples of the posterior distribution. Regarding potential detrimental influence of MRI on PET, an issue may arise when a single MRI segment encompasses several PET segments: especially if these segments are small, slight averaging in the PET image may occur, as may be observed in the simulation (lesion). If several MRI segments match a uniform PET region, the PET intensity should not be impaired. In general, very small segments with very few PET counts suffer from lack of observation, hence they are more influenced by the wide-range prior and more difficult to sample. A possible improvement regarding segmentation could be a finer, preferably automatic tuning of the balance between MRI and PET influence on the segmentation.

The Gibbs sampler had convergence difficulties and several runs were needed, but this issue is being investigated. Whenever a prior is introduced in a model, its characteristics and parameters need to be chosen with care and with reality in mind. In our prior, the influence of the intensity prior parameters was rather small compared to the influence of the segmentation part of the model. It should be noted that deterministic methods for solving inverse problem, such as MLEM, might also be viewed as probabilistic methods with non-informative priors.

The posterior distribution reveals uncertainty information from several sources: from the prior distribution of intensity and segmentation, from intensity observations from PET data and from segmentation observations from both PET and MRI data, so the intepretation of credible intervals is not straightforward.

Further tests shall be performed for refining and automating the choice of parameters, and for a more thorough interpretation of uncertainty.

In conclusion, we proposed a new method for PET image and uncertainty reconstruction including anatomical information. The preliminary results are promising, so further tests are being performed and improvements are being investigated.

This work is supported by the Lidex-PIM project funded by the IDEX Paris-Saclay, ANR-11-IDEX-0003-02. Thanks to Catherine Chiron for kindly providing data from the EPIPED research protocol.

References

[1] *CASToR - Customizable and Advanced Software for Tomographic Reconstruction*. Mar 2017. URL http://www.castor-project.org/.

[2] B. Bai, Q. Li, and R. M. Leahy. Magnetic resonance-guided positron emission tomography image reconstruction. *Seminars in Nuclear Medicine*, 43(1): 30–44, Jan. 2013.

[3] E. Barat, C. Comtat, T. Dautremer, T. Montagu, and R. Trebossen. A nonparametric bayesian approach for pet reconstruction. In *2007 IEEE Nuclear Science Symposium Conference Record*, pages 4155–4162, 2007.

[4] D. M. Blei and P. I. Frazier. Distance dependent chinese restaurant process. *Journal of Machine Learning Research*, 12:2461–2488, 2011.

[5] D. M. Higdon, J. E. Bowsher, V. E. Johnson, T. G. Turkington, D. R. Gilland, and R. J. Jaszczak. Fully bayesian estimation of gibbs hyperparameters for emission computed tomography data. *IEEE Transactions on Medical Imaging*, 16(5):516–526, Oct. 1997.

[6] H. Jeffreys. *The Theory of Probability*. 1961.

[7] J. Qi and R. M. Leahy. Iterative reconstruction techniques in emission computed tomography. *Physics in Medicine and Biology*, 51:541–578, 2006.

[8] A. Sitek. Reconstruction of emission tomography data using origin ensembles. *IEEE Transactions on Medical Imaging*, 30(4):946–956, Apr. 2011.

[9] S. Stute, C. Tauber, C. Leroy, M. Bottlaender, V. Brulon, and C. Comtat. Analytical simulations of dynamic pet scans with realistic count rates properties. In *2015 IEEE Nuclear Science Symposium and Medical Imaging Conference (NSS/MIC)*, pages 1–3, Oct 2015.

[10] I. S. Weir. Fully bayesian reconstructions from single-photon emission computed tomography data. *Journal of the American Statistical Association*, 92(437):49–60, Dec. 1995.